Estimating the occurrence of labial bone perforation and implantation into the maxillary sinus maxillary premolars based on the morphology of maxillary premolars: A clinical study

Zhuo-lin Kong
First Affiliated Hospital of Wenzhou Medical University
Yun-yun Tu
First Affiliated Hospital of Wenzhou Medical University
Dong-qian Xu
First Affiliated Hospital of Wenzhou Medical University
Xi Ding (dingxi@wzhospital.cn)
First Affiliated Hospital of Wenzhou Medical University

Research Article

Keywords: Cone-beam computed tomography, Dental implants, maxillary premolars, Virtual implant planning

Posted Date: February 16th, 2023

DOI: https://doi.org/10.21203/rs.3.rs-2565280/v1

Additional Declarations: No competing interests reported.

Estimating the occurrence of labial bone perforation and implantation into the maxillary sinus maxillary premolars based on the morphology of maxillary premolars: A clinical study

Zhuo-lin Kong[1] • Yun-yun Tu[2] • Dong-qian Xu[1] • Xi Ding[1]

[1]Department of Stomatology, The First Affiliated Hospital of Wenzhou Medical University, Wenzhou, Zhejiang, PR China.

[2]Department of Neonatology, The First Affiliated Hospital of Wenzhou Medical University, Wenzhou, Zhejiang, PR China.

Corresponding author:

Xi Ding

Professor, Department of Stomatology

The First Affiliated Hospital of Wenzhou Medical University

Nanbaixiang Ouhai District, Wenzhou Zhejiang 325000

PR China

Email: dingxizj@hotmail.com

ABSTRACT

Objectives The purpose of this study was to investigate the occurrence of labial bone perforation (LBP) and implantation into the maxillary sinus between various tooth-alveolar classifications with respect to the crown axis in maxillary premolars.

Material and methods Cone beam computed tomography (CBCT) of 399 participants were analyzed to determine the probability of LBP and implantation into the maxillary sinus when associated with variables that included tooth position and tooth-alveolar classification.

Results The morphology in the maxillary premolars was classified as straight, oblique, or boot-shaped. The first premolars were 62.3% straight, 37.0% oblique, and 0.8% boot-shaped and LBP occurred in 4.2% straight, 54.2% oblique, and 83.3% boot-shaped first premolars when the virtual implant was 3.5×10 mm. When the virtual implant was 4.3×10 mm, LBP occurred in 8.5% , 68.5% and 83.3% first premolars, respectively. The second premolars were 92.4% straight, 7.5% oblique, and 0.1% boot-shaped and LBP occurred in 0.5% straight , 33.3% oblique, and 0% boot-shaped, respectively, when the virtual implant was 3.5×10 mm; and LBP occurred in 1.3%, 53.3% and 100% second premolars, respectively, when the virtual implant was 4.3×10 mm.

Conclusions When an implant is placed in the long axis of a maxillary premolar, the tooth position and tooth-alveolar classification should be considered when assessing the risk of LBP. Attention should be paid to the implant direction, diameter, and length in the oblique and boot-shaped maxillary premolars.

Clinical relevance Preoperative CBCT needs to be used to reduce LBP in the maxillary premolars, especially when oblique or boot-shaped.

Keywords Cone-beam computed tomography • Dental implants • maxillary premolars • Virtual implant planning

Introduction

When placing implant in the maxillary premolar location, buccal perforation, dehiscence, or both, may occur because of a thin labial wall and buccal concavity. Perforation may lead to difficulty in achieving primary implant stability, an unsatisfactory esthetic outcome, and a high implant failure rate[1,2]. The maxillary sinus is located within the maxillary body, close to the maxillary posterior teeth. Complications during the maxillary posterior teeth implantation, such as maxillary sinus perforation or maxillary sinus infection, may occur if clinicians do not fully understand the anatomical relationship between the alveolar bone and the maxillary sinus[3].The positions and angulations of the central incisors, lateral incisors, and canines have been classified with reference to the alveolar bone[4,5] to guide anterior implant locations. However, similar classifications about maxillary premolar locations are lacking.

Contemporary implant treatment has focused on improving esthetics and ensuring long-term stability[6] with restoration-driven treatment planning starting with determining the location of the restoration before determining the implant position[6]. However, restoration-driven treatment can be challenging because of the perforation risk, especially in esthetic areas between the maxillary first or second premolars[7]. Data on maxillary premolar implantation adopting the restoration-driven treatment plan are lacking. Therefore, a study of the distribution of labial bone perforation (LBP) in maxillary premolars is needed to produce a classification of the maxillary

premolar morphology to guide maxillary premolar implantation.

Cone beam computed tomography (CBCT) has become popular in dentistry, yielding less radiation than conventional CT scanning and producing accurate images with rapid scan times[8-12]. Virtual implants can be used to simulate buccal perforation following the crown axis from CBCT scanning. Computer-guided implant planning may allow for an accurate evaluation of the implant location on CBCT images, taking on the restoration-driven approach[5,13-14].

Combined with the restoration-driven principle, the crown axis has been innovatively used as the implant direction to study the angle between the long axis of the tooth crown and alveolar bone, residual buccal bone thickness, LBP, and implantation into the maxillary sinus after virtual implantation[13]. It was possible that LBP occurred in maxillary premolars when virtually implantation according to the restoration-driven principle. This study aimed to classify the morphology of maxillary premolars to guide dental implantation treatment planning.

MATERIAL AND METHODS

This study was approved by the Institutional Review Board of the First Affiliated Hospital of Wenzhou Medical University and was conducted from July 2019 to August 2021. The minimum sample size of 385 participants for the study was determined using the cross sectional studies with $4Z_{\alpha}^{2}P(1-P)/W^{2}$ where W is the width of confidence intervals at 1%, and Z_{α} is the 95% confidence interval at 1.96.Inclusion criteria for the images in this study were a clear view of the maxillae without scattering artifacts from metal restorations, adults $\geqslant$18 years with complete

maxillary dentition, no obvious maxillary crowding or spacing, no history of periodontitis, and no pathology present in the region of interest.

All images were obtained using the same CBCT machine (3D eXam, KaVo) with a minimum filtration equivalent of 120 kVp, scanning time of 4.8 seconds, tube current of 3 to 7 mA, 320 scanning layers, and thickness of each layer of 0.3 mm. The scans used in this study were selected from the CBCT database and were not specifically acquired for the study. Data were saved in the digital imaging and communications in medicine (DICOM) format. The DICOM file for each individual was transferred to a desktop computer equipped with an implant-planning software program (NobelClinician, Nobel Biocare). The scan was oriented such that the maxilla was symmetrical, and the palatal plane was parallel to the ground.

The long axis of the crown was determined by connecting the buccolingual midpoint at the cementoenamel junction and central fossa (Fig. 1). The long axis of the alveolar bone represented the line running through the labiopalatal midpoint of the alveolar bone (Fig. 2). Tapered implants (3.5×10 mm, 4.3×10 mm Nobel Active; Nobel Biocare) were placed virtually in the selected central sites. Virtual implant placement was then completed following a restoration-driven approach, with the screw access located in the central fossa of the premolar crowns along its long axis. The implant platform was positioned at the crestal level apicocoronally (Fig. 1). After the virtual implant had beenplaced, measurements were made in the midsagittal plane of the virtual implant and the relationship between the alveolar bone and the virtually placed implant evaluated.

Measurements were made at 3 levels as described by Sarnachiaro et al[15]: L1, coronal level;

L2, middle level; L3, apical level at the time of implant placement. The coronal level corresponded to the implant platform, and the middle level corresponded to the implant half-length, where the apical level was at the implant apex. At each level, 2 reference points were identified: the plate's most buccal or palatal point and the implant contact point. A straight line connected the points. The distance between the 2 points at each level was measured (B1, B2, B3, P1, P2, P3). The tooth-alveolar angle was defined as between the long axis of the crown and alveolar bone (Fig. 3). Distance EF was from the virtual implant bottom to the maxillary sinus floor (Fig. 3).

A single examiner (Z.K.) performed all measurements. The intra-examiner reliability was 0.921 for duplicate examinations from 2 randomly selected premolars after virtually implantation3 days apart. The measurements were repeated 3 times, and the mean values were used. All measurements were presented as mean ±standard deviation (SD). The chi-squared test and 1-way ANOVAs were used to examine differences in categorical variables, including the frequency distribution of different types of implant angulation, LBP, and implantation into the maxillary sinus in maxillary premolars. Independent *t* tests were used to compare the mean values of B1, B2, B3, P1, P2, P3, and the tooth-alveolar angle at non-perforation and perforation sites. Binary logistic regression modelling was used to determine if the odds ratios of variables made an important contribution to the probability of LBP and implantation into the maxillary sinus. Statistical analysis was performed using a statistical software program (SPSS Statistics v17.0, SPSS Inc) (α=.05).

RESULTS

A representative pair of straight shapes are shown in Figure 4. For both Type A and B, the long axes of the crowns were parallel to that of the alveolar bone. However, a wider alveolar bone was observed in Type A than Type B.A representative pair of oblique shapes are shown in Figure 5. Unlike in Figure 4, the long axes of the crowns were inclined relative to that of the alveolar bone, but similarly to Figure 4, a wider alveolar bone was observed in Type A than Type B.A representative boot shape is shown in Figure 6. A concavity was observed in the middle part of the alveolar bone.

After application of the inclusion criteria, a total of 399 participants, 201 men and 198 women, with 1596 teeth were available for further analysis. Table 1 showed the frequency distributions of the tooth-alveolar classification in maxillary premolars. When the virtual implant was 3.5×10 mm, perforation was more likely to occur in the first premolars (23.3%) compared with the second premolars (3.0%) (Table 2). LBP occurred in straight, oblique, and boot-shaped first and second premolars (Table 3). When the virtual implant was 4.3×10 mm, LBP was more likely to occur in the first premolars (31.2%) compared with the second premolars (5.4%) (Table 4). LBP occurred in the straight, oblique, and boot-shaped first and second premolars (Table 5).

The tooth-alveolar angle in the perforation group was significantly higher than that in the non-perforation group (P<.001) (Table 6).The probability of LBP was significantly different between each tooth type (P<.001) (Table 7). The distance was smaller in the second premolars than in the first premolars (P<.001) (Table 8). The distance was lower in the perforation group than in the non-perforation group (P<.001).

After adjusting for the right or left side, sex, age, tooth-alveolar classification, and tooth-alveolar angle, the odds of LBP in virtually placed implants in the first premolars were 2.30 times (95% confidence interval [CI], 1.35–3.91; *P*=.002) higher than the odds in the second premolars, and the odds of virtually touching the maxillary sinus floor in the second premolars were 4.36 times (95% CI, 2.73–6.97; *P*<.001) higher than the odds in the first premolars.

DISCUSSION

The perforation rates of various morphologies in maxillary premolars were significantly higher for oblique and boot shapes. Clinically, in maxillary premolar implantation, buccal perforation, dehiscence, or both may occur because of a thin labial wall and buccal concavity. Studies showed that a thinner buccal bone wall was found in upper anterior teeth, first premolars, and second premolars[16]. The buccal bone wall also differed between multiple and single roots in first and second premolars. Buccal concavity may appear due to the morphology of the maxilla or due to other causes, such as root pathology or periapical infections. Data on maxillary premolar implantation adopting the restoration-driven treatment plan are lacking. Therefore, this study analyzed CBCT data to help make decisions regarding maxillary premolar implant replacement. Nowadays, CBCT has become a conventional technique for clinical diagnosis and implant planning owing to its high accuracy, low radiation dose, and convenience[8,17-18].

In this study, maxillary premolars were categorized according to the tooth-alveolar shape as follows: straight (the long axis of the crown was parallel to the long axis of the alveolar bone), oblique (the long axis of the crown was inclined relative to the long axis of the alveolar bone),

and boot-shaped (the middle part of the alveolar bone was concave). Among the three shapes, the straight shape was the category with the highest probability of non-perforation compared to that of the oblique and the boot-shaped group. Therefore, the straight shape, where dental implantation along the crown axis, was the most suitable morphology. An appropriate implant diameter should be decided based on the width of the alveolar bone for Type B of the straight shape. For the oblique shape, implant direction and length should be considered during surgery. In particular, the proper implant direction, diameter, and length should be considered in Type B of the oblique shape. If necessary, adjustment of implant angulation or a tapered implant may be beneficial for preventing LBP. The boot shape was the most difficult to implant, and attention should be paid to its implant direction, diameter, and length. If necessary, adjustment of the implant angulation using a narrow tapered implant may be beneficial for preventing LBP. The incidence of perforation significantly increased in oblique and boot shape. It was also found that tooth-alveolar angle larger than 30 degrees might cause LBP. The oblique and boot shape of 37.8% in the first premolars and 7.6% in the second premolars needed to be paid attention to the direction of implantation. If the site exhibited a high risk of LBP for oblique and boot-shaped, a guide plate was needed to determine the implantation direction. A thin labial plate could also lead to LBP and affect the amount of labial thickness reconstruction[17]. This requires clinicians to consider treatment options to reduce the risk of LBP. Placing bone grafts, absorbable membranes, socket shield technique, and immediate implant placement without delay were used to improve labial plate thickness[15,19-20].

In previous studies, root position was assessed only in the maxillary anterior teeth, and few

provided information on the spatial relationship between the root and the alveolar bone[4,21-22]. Lau et al used CBCT to classify maxillary central incisors by analyzing the position and angulation of the teeth[21]. Most of the central incisors were type B (78.8%), while 19.4% and 1.8% were type M and P, respectively[21]. Kan et al evaluated the association between the position of maxillary anterior teeth and their osseous housing, categorizing them as class I–IV[4]. The frequency distribution of the sagittal root position of maxillary anterior teeth indicated that 81.1%, 6.5%, 0.7% and 11.7% were classified as class I, II, III, and IV, respectively[4]. Sung et al determined that perforation was most likely to occur in canine teeth (94.1%) compared to central (85.6%) or lateral incisors (71.9%)[5]. LBP was most likely to occur in maxillary anterior teeth than in maxillary premolars. This difference can be attributed to the interaction between study design, classification system, tooth positions, dental condition, and racial and ethnic causes.

The "crown-down" approach for implantation was clinically unfeasible; therefore, virtual implants were used to simulate buccal perforations following the crown axis. Computer-guided implant planning may allow an accurate evaluation of the implant location on CBCT. Several studies have used virtual implants to study LBP[5,13], nasopalatine canal perforations (NPC) [14,23], and lingual perforations[6]. Till date, few studies were reported to utilize virtual implants to analyze LBP in maxillary premolars.

This study began with a restoration-driven treatment plan and drew on the spatial relationship between the tooth and alveolar bone in maxillary premolars[4-5,20]. The proportion and influencing factors of buccal perforation in the maxillary premolars were studied using

virtual implants.

However, the results and classifications in this study lacked alveolar bone atrophy after tooth loss. Tooth extraction and trauma to hard tissues are followed by pronounced resorption, particularly of the buccal bone plate[13,17,23]. These changes may be due to the loss of periodontal ligaments and continuous trauma, particularly to the cheekbone plate[24]. Future research should focus on alveolar bone atrophy, which may refine the classification of the posterior maxillary morphology.

CONCLUSIONS

Based on the findings of this study, the following conclusions were drawn:

1. The morphology of maxillary premolars was classified into three types (straight, oblique, and boot-shaped) based on CBCT scanning.

2. LBP was common in the first maxillary premolars when an implant was placed according to the crown axis, less seen in second maxillary premolars. The perforation rate was significantly higher in the oblique and the boot-shaped types than the straight shape type. Attention should be paid to the implant direction, diameter, and length in the oblique and boot-shaped types.

3. Preoperative CBCT should be considered to estimate the morphology and LBP in maxillary premolars.

Acknowledgements Not applicable

CRediT Conceptualization Xi Ding; Methodology: Yun-yun Tu, Formal analysis and

investigation: Zhuo-lin Kong, Writing - original draft preparation: Zhuo-lin Kong; Writing - review and editing: Dong-qian Xu, Funding acquisition: Zhuo-lin Kong, Xi Ding; Resources: Zhuo-lin Kong, Xi Ding; Supervision: Xi Ding.

Funding This study was funded by Wenzhou Major Scientific and Technological Innovation Project (ZY2022022, Y20220373).

Data availability The data presented in this study are available on reasonable request from the corresponding author.

Declarations

Ethics approval and consent to participate This study was reviewed and approved by the Research Ethics Committee of the First Affiliated Hospital of Wenzhou Medical University (Issuing Number: KY2022-R146) and in full accordance with the world medical Declaration of Helsinki. Written informed consent was obtained from all the participants.

Consent for publication Not applicable.

Conflict of Interest The authors declare that they have no conflict of interest.

REFERENCES

1. Hämmerle CH, Araújo MG, Simion M. Osteology Consensus Group 2011 (2012) Evidence-based knowledge on the biology and treatment of extraction sockets. Clin Oral Implants Res 23:80–82. https://doi.org/10.1111/j.1600-0501.2011.02370.x

2. den Hartog L, Slater JJ, Vissink A, Meijer HJ, Raghoebar GM (2008) Treatment outcome of immediate, early and conventional single-tooth implants in the aesthetic zone: A systematic review to survival, bone level, soft-tissue, aesthetics and patient satisfaction. J ClinPeriodontol 35:1073–1086. https://doi.org/10.1111/j.1600-051X.2008.01330.x

3. Yang SM, Kye SB (2014) Location of maxillary intraosseous vascular anastomosis based on the tooth position and height of the residual alveolar bone: Computed tomographic analysis. J Periodontal Implant Sci 44:50–56. https://doi.org/10.5051/jpis.2014.44.2.50

4. Kan JY, Roe P, Rungcharassaeng K, Patel RD, Waki T, Lozada JL, Zimmerman G (2011) Classification of sagittal root position in relation to the anterior maxillary osseous housing for immediate implant placement: A cone beam computed tomography study. Int J Oral Maxillofac Implants 26:873–876.

5. Sung CE, Cochran DL, Cheng WC, Mau LP, Huang PH, Fan WH, Shieh YS, Huang RY (2015) Preoperative assessment of labial bone perforation for virtual immediate implant surgery in the maxillary esthetic zone: A computer simulation study. J Am Dent Assoc 146:808–819. https://doi.org/10.1016/j.adaj.2015.04.007

6. Chan HL, Benavides E, Yeh CY, Fu JH, Rudek IE, Wang HL (2011) Risk assessment of lingual plate perforation in posterior mandibular region: A virtual implant placement study using

cone-beam computed tomography. J Periodontol 82:129–135. https://doi.org/10.1902/jop.2010.100313

7. Testori T, Weinstein T, Scutellà F, Wang HL, Zucchelli G (2018) Implant placement in the esthetic area: Criteria for positioning single and multiple implants. Periodontol 2000 77:176–196. https://doi.org/10.1111/prd.12211

8. Arai Y, Tammisalo E, Iwai K, Hashimoto K, Shinoda K (1999) Development of a compact computed tomographic apparatus for dental use. Dentomaxillofac Radiol 28:245–248. https://doi.org/10.1038/sj/dmfr/4600448

9. Scarfe WC, Farman AG, Sukovic P (2006) Clinical applications of cone-beam computed tomography in dental practice. J Can Dent Assoc 72:75–80.

10. Chau AC, Fung K (2009) Comparison of radiation dose for implant imaging using conventional spiral tomography, computed tomography, and cone-beam computed tomography. Oral Surg Oral Med Oral Pathol Oral Radiol Endod. 107:559–565. https://doi.org/10.1016/j.tripleo.2008.11.009

11. Yildiz S, Bayar GR, Guvenc I, Kocabiyik N, Cömert A, Yazar F (2015) Tomographic evaluation on bone morphology in posterior mandibular region for safe placement of dental implant. Surg Radiol Anat 37:167–173. https://doi.org/10.1007/s00276-014-1351-1

12. Quirynen M, Mraiwa N, van Steenberghe D, Jacobs R (2003) Morphology and dimensions of the mandibular jaw bone in the interforaminal region in patients requiring implants in the distal areas. Clin Oral Implants Res 14:280–285. https://doi.org/10.1034/j.1600-0501.2003.140305.x

13. Chan HL, Garaicoa-Pazmino C, Suarez F, Monje A, Benavides E, Oh TJ, Wang HL (2014)

Incidence of implant buccal plate fenestration in the esthetic zone: A cone beam computed tomography study. Int J Oral Maxillofac Implants 29:171–177. https://doi.org/10.11607/jomi.3397

14. Alkanderi A, Al Sakka Y, Koticha T, Li J, Masood F, Suárez-López Del Amo F (2020) Incidence of nasopalatine canal perforation in relation to virtual implant placement: A cone beam computed tomography study. Clin Implant Dent Relat Res 22:77–83. https://doi.org/10.1111/cid.12852

15. Sarnachiaro GO, Chu SJ, Sarnachiaro E, Gotta SL, Tarnow DP (2016) Immediate implant placement into extraction sockets with labial plate dehiscence defects: A clinical case series. Clin Implant Dent Relat Res 18:821–829. https://doi.org/10.1111/cid.12347

16. López-Jarana P, Díaz-Castro CM, Falcão A, Falcão C, Ríos-Santos JV, Herrero-Climent M (2018) Thickness of the buccal bone wall and root angulation in the maxilla and mandible: An approach to cone beam computed tomography. BMC Oral Health 18:194. https://doi.org/10.1186/s12903-018-0652-x

17. Covani U, Ricci M, Bozzolo G, Mangano F, Zini A, Barone A (2011) Analysis of the pattern of the alveolar ridge remodelling following single tooth extraction. Clin Oral Implants Res 22:820–825. https://doi.org/10.1111/j.1600-0501.2010.02060.x

18. Blanco J, Alonso A, Sanz M (2005) Long-term results and survival rate of implants treated with guided bone regeneration: A 5-year case series prospective study. Clin Oral Implants Res 16:294–301. https://doi.org/10.1111/j.1600-0501.2005.01106.x

19. Tan-Chu JH, Tuminelli FJ, Kurtz KS, Tarnow DP (2014) Analysis of buccolingual

dimensional changes of the extraction socket using the "ice cream cone" flapless grafting technique. Int J Periodontics Restorative Dent 34:399–403. https://doi.org/10.11607/prd.1605

20. Hürzeler MB, Zuhr O, Schupbach P, Rebele SF, Emmanouilidis N, Fickl S (2010) The socket-shield technique: A proof-of-principle report. J Clin Periodontol 37:855–862. https://doi.org/10.1111/j.1600-051X.2010.01595.x

21. Lau SL, Chow J, Li W, Chow LK (2011) Classification of maxillary central incisors-implications for immediate implant in the esthetic zone. J Oral Maxillofac Surg 69:142–153. https://doi.org/10.1016/j.joms.2010.07.074

22. Vera C, De Kok IJ, Reinhold D, Limpiphipatanakorn P, Yap AK, Tyndall D, Cooper LF (2012) Evaluation of buccal alveolar bone dimension of maxillary anterior and premolar teeth: A cone beam computed tomography investigation. Int J Oral Maxillofac Implants 27:1514–9.

23. Jia X, Hu W, Meng H (2015) Relationship of central incisor implant placement to the ridge configuration anterior to the nasopalatine canal in dentate and partially edentulous individuals: A comparative study. Peer J 3:e1315. https://doi.org/10.7717/peerj.1315

24. Araújo MG, Sukekava F, Wennström JL, Lindhe J (2005) Ridge alterations following implant placement in fresh extraction sockets: An experimental study in the dog. J Clin Periodontol 32:645–652. https://doi.org/10.1111/j.1600-051X.2005.00726.x

TABLES

Table 1. Frequency distribution of tooth-alveolar classification in maxillary premolars

Variable	Straight shape				Oblique shape				Boot shape		*P*
	Type A		Type B		Type A		Type B				
	n	%	n	%	n	%	n	%	n	%	
Right	627	78.6	4	0.5	132	16.5	33	4.1	2	0.3	.320
Left	597	74.8	6	0.8	146	18.3	44	5.5	5	0.6	
1st premolar	492	61.7	5	0.6	240	30.1	55	6.9	6	0.8	<.001
2nd premolar	732	91.7	5	0.6	38	4.8	22	2.8	1	0.1	
1st premolar, right	255	63.9	3	0.8	116	29.1	23	5.8	2	0.5	<.001
1st premolar, left	237	59.4	2	0.5	124	31.1	32	8.0	4	1.0	
2nd premolar, right	372	93.2	1	0.3	16	4.0	10	2.5	0	0	
2nd premolar, left	360	90.2	4	1.0	22	5.5	12	3.0	1	0.3	
Total	1224	76.7	10	0.6	278	17.4	77	4.8	7	0.4	

Table 2. Frequency distribution of labial bone perforation in maxillary premolars (3.5×10 mm implant)

Variable	Perforation (Pe)		Non-perforation (NP)		*P*
	n	%	n	%	
Right	91	11.4	707	88.6	.010
Left	119	14.9	679	85.1	
1st premolar	186	23.3	612	76.7	<.001
2nd premolar	24	3.0	774	97.0	
1st premolar, right	83	20.8	316	79.2	.019
1st premolar, left	103	25.8	296	74.2	
2nd premolar, right	8	2.0	391	98.0	
2nd premolar, left	16	4.0	383	96.0	
Total	210	13.2	1386	86.8	

Table 3. Distribution of LBP according to tooth-alveolar classification in maxillary premolars (3.5×10 mm implant)

Variable	Straight shape				Oblique shape				Boot shape	
	Type A		Type B		Type A		Type B			
	Pe	NP	Pe	NP	Pe	NP	Pe	NP	Pe	NP
Right	10	618	3	0	53	79	23	10	2	0
Left	11	586	1	5	75	71	29	15	3	2
1st premolar	18	474	3	2	119	121	41	14	5	1
2nd premolar	3	730	1	3	9	29	11	11	0	1
14	9	246	3	0	52	64	17	6	2	0
24	9	228	0	2	67	57	24	8	3	1
15	1	372	0	0	1	15	6	4	0	0
25	2	358	1	3	8	14	5	7	0	1
Total	21	1204	4	5	128	150	52	25	5	2

Pe, perforation group; NP, non-perforation group.

Table 4. Frequency distribution of labial bone perforation in maxillary premolars (4.3×10 mm implant)

Variable	Perforation		Non-perforation		*P*
	n	%	n	%	
Right	119	14.9	679	85.1	<.001
Left	173	21.7	625	78.3	
1st premolar	249	31.2	549	68.8	<.001
2nd premolar	43	5.4	755	94.6	
1st premolar, right	105	26.3	294	73.7	<.001
1st premolar, left	144	36.1	255	63.9	
2nd premolar, right	14	3.5	385	96.5	
2nd premolar, left	29	7.3	370	92.7	
Total	292	18.3	1304	81.7	

Table 5. Distribution of LBP according to tooth-alveolar classification in maxillary premolars (4.3×10 mm implant)

Variable	Straight shape				Oblique shape				Boot shape	
	Type A		Type B		Type A		Type B			
	Pe	NP	Pe	NP	Pe	NP	Pe	NP	Pe	NP
Right	20	608	0	3	72	60	25	8	2	0
Left	30	567	2	4	100	46	37	7	4	1
1st premolar	41	451	1	4	156	84	46	9	5	1
2nd premolar	9	724	1	3	16	22	16	6	1	0
14	16	239	0	3	69	47	18	5	2	0
24	25	212	1	1	87	37	28	4	3	1
15	4	369	0	0	3	13	7	3	0	0
25	5	355	1	3	13	9	9	3	1	0
Total	50	1175	2	7	172	106	62	15	6	1

Pe, perforation group; NP, non-perforation group

Table 6. Comparisons of tooth-alveolar angle in labial bone perforation and non-perforation sites in maxillary premolars

Variable	Mean ± SD	*P*	Perforation, mean ± SD		*P* (Pe vs. NP)
			Yes	No	
Left	20.9±8.52°	.035	30.5±5.75°	19.1±7.72°	<.001
Right	19.5±9.23°		31.5±6.63°	17.9±8.30°	<.001
1st premolar	24.1±8.39°	<.001	31.3±6.09°	21.9±7.72°	<.001
2nd premolar	16.2±7.57°		28.3±5.99°	15.8±7.24°	<.001
14	23.4±8.96°	<.001	31.7±6.49°	21.2±8.19°	<.001
24	24.9±7.70°		31.0±5.73°	22.7±7.11°	<.001
15	15.5±7.68°		29.4±7.48°	15.2±7.38°	<.001
25	17.0±7.38°		27.8±5.11°	16.4±7.03°	<.001

Pe, perforation group; NP, non-perforation group.

Table 7. Frequency distribution of maxillary sinus perforation in maxillary premolars

Variable	Perforation		Non-perforation		*P*
	n	%	n	%	
Right	79	9.9	719	90.1	.132
Left	61	7.6	737	92.4	
1st premolar	23	2.9	775	97.1	<.001
2nd premolar	117	14.7	681	85.3	
1st premolar, right	14	3.5	385	96.5	<.001
1st premolar, left	9	2.3	390	97.7	
2nd premolar, right	65	16.3	334	83.7	
2nd premolar, left	52	13.0	347	87.0	
Total	140	8.8	1456	91.2	

Table 8. Distance (mm) from bottom of virtual implant (10 mm) to maxillary sinus floor in maxillary premolar in straight shape

Variable	Mean ± SD	*P*	Perforation, mean ± SD		*P* (Pe vs. NP)
			Yes	No	
Left	4.00±3.43	.708	-1.55±0.93	4.72±2.91	<.001
Right	3.92±3.49		-1.42±0.90	4.79±2.94	<.001
1st premolar	5.03±3.18	<.001	-1.29±0.67	5.41±2.85	<.001
2nd premolar	3.34±3.46		-1.52±0.95	4.32±2.91	<.001
1st premolar, right	4.90±3.10	<.001	-1.20±0.65	5.30±2.80	<.001
1st premolar, left	5.22±3.22		-1.43±0.67	5.54±2.92	<.001
2nd premolar, right	3.37±3.57		-1.47±0.94	4.45±3.00	<.001
2nd premolar, left	3.31±3.35		-1.57±0.96	4.20±2.82	<.001

Pe, perforation group; NP, non-perforation group.

FIGURES

Figure 1. Determination of long axis of crown (L_a). Long axis of crown was determined by connecting buccolingual midpoint (C) at cementoenamel junction and central fossa (D).

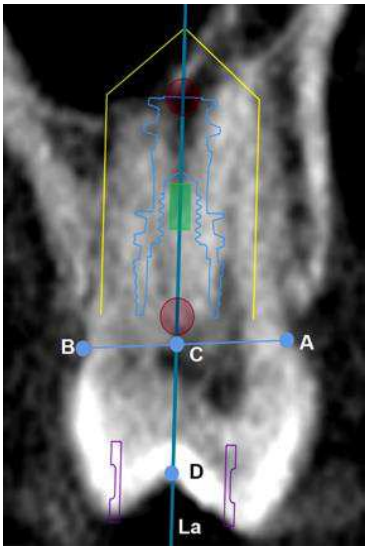

Figure 2. Determination of long axis of alveolar bone (L_b). Long axis of alveolar bone represents line running through labiopalatal midpoint of alveolar bone. Tooth-alveolar angle (∠1): angulation between long axis of crown (L_a) and long axis of alveolar bone (L_b).

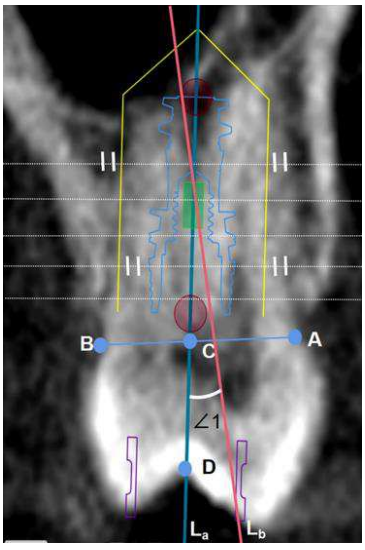

Figure 3. Data measurement. Labial/palatal bone thickness between alveolar bone and virtually placed implant at coronal, middle, and apical levels (B1, B2, B3, P1, P2, P3). Distance (EF) from virtual implant bottom to maxillary sinus floor.

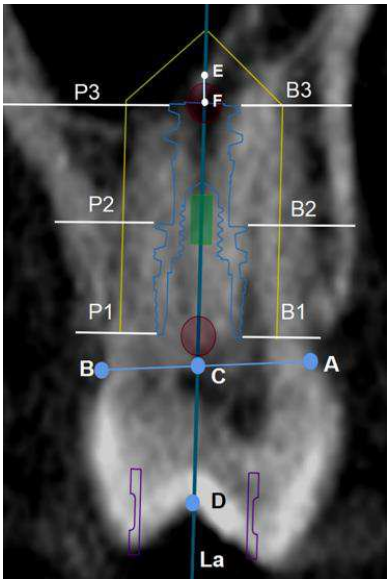

Figure 4. (A) Radiographic image of type A straight shape. (B) Graphic illustration of type A straight shape. (C) Cross-sectional CBCT image demonstrating dental implant insertion in type A straight shape. (D) Radiographic image of type B straight shape. (E) Graphic illustration of type B straight shape. (F) Cross-sectional CBCT image demonstrating dental implant insertion in type B straight shape.

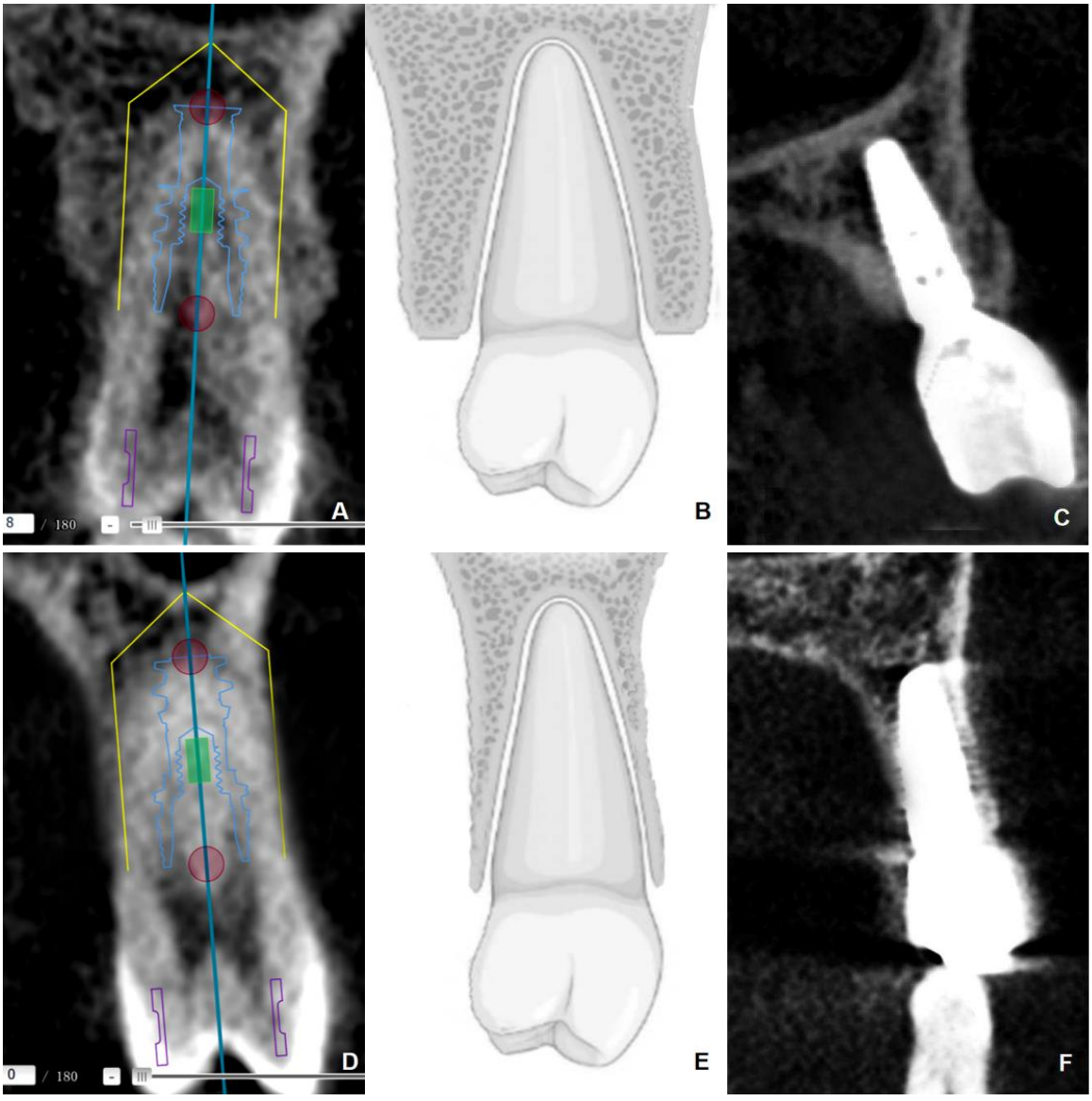

Figure 5. (A) Radiographic image of type A oblique shape. (B) Graphic illustration of type A oblique shape. (C) Cross-sectional CBCT image demonstrating dental implant insertion in type A oblique shape. (D) Radiographic image of type B oblique shape. (E) Graphic illustration of type B oblique shape. (F) Cross-sectional CBCT image demonstrating dental implant insertion in type B oblique shape.

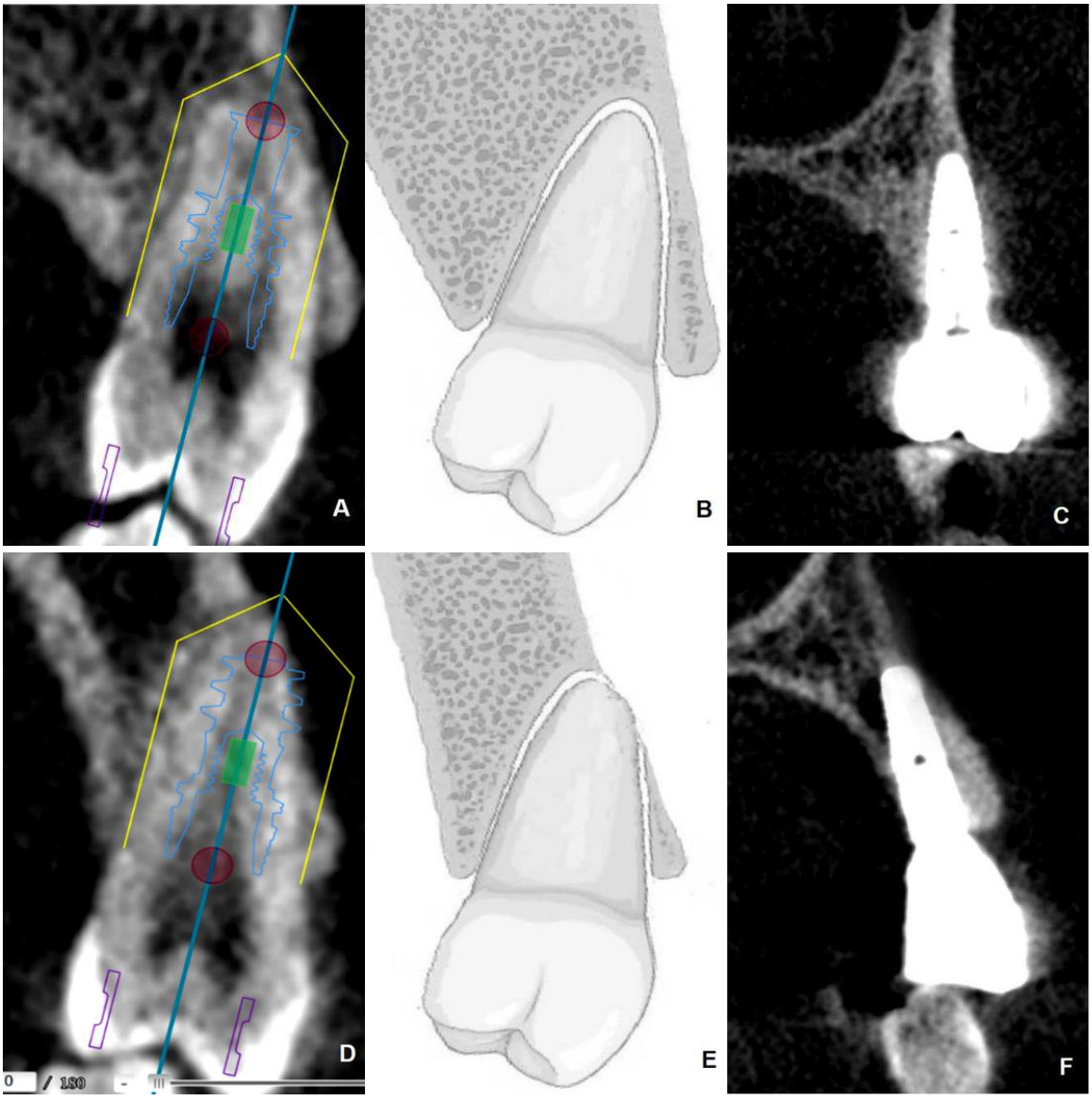

Figure 6. (A) Radiographic image of boot shape. (B) Graphic illustration of boot shape. (C) Cross-sectional CBCT image demonstrating dental implant insertion in boot shape.